Random-Matrix Theory of Quantum Transport in Topological Superconductors

Praveen Sriram
Department of Applied Physics, Stanford University, Stanford, CA 94305
(Dated: June 23, 2020)

Submitted as coursework for PH470, Stanford University, Spring 2020

The theory of random matrices first made its appearance in physics to study atomic nuclei. It has since been used to study universal transport properties of quantum dots and nanowires. The discovery of topological phases in condensed matter, with the emergence of Majorana zero modes at the ends of a topological superconductor provide a new arena for the application of random-matrix theory. The Hamiltonian and scattering matrix ensembles for the tenfold-way classification of symmetry classes is discussed. It is observed that the topological quantum number is uniquely determined by the reflection matrix at the Fermi level of a chaotic system. Percepts from random-matrix theory can also be used to probe non-distinguishable transport signatures of the trivial and non-trivial phases. Recent developments and experimental signatures of the non-trivial phase are reviewed, with a focus on electrical conduction.

I. INTRODUCTION

Random-matrix theory (RMT) is the study of the spectral properties of large matrices with randomly distributed elements. Given the probability distribution of the matrices, correlation functions of its eigenvalues and eigenvectors are derived. These correlation functions are then used to compute physical observables of the system. Random matrices were first employed in physics in the 1950s[1], to explain the statistical properties of nuclear reactions. Since then, RMT has been widely applied in various fields of physics, including condensed matter physics, where RMT describes the universal properties of disordered metals and superconductors.

The development of a random-matrix theory of quantum transport was fuelled by two developments in the 1980s. The first was the discovery of the universal description of chaotic systems in terms of the Wigner-Dyson ensemble (Sec. IV B). Soon after, a relation between the universal properties of large random matrices and universal conductance fluctuations (UCF) in disordered conductors was discovered. In this report, we are concerned with the transport properties of mesoscopic systems – an intermediate scale between the microscopic and macroscopic. These systems are small enough that their quantum mechanical phase-coherence is preserved, but large enough that a statistical description is complete. Universal transport properties are independent of the microscopic description of the system, such as potential landscape, disorder strength and system size. Random matrix-theory links these universal features with the universality of correlation functions of transmission eigenvalues, dependent only on the presence or absence of certain symmetries. This approach is powerful, since transmission matrix determines every linear-response transport statistic, and not just the conductance. Furthermore, this is a non-perturbative theory, and hence provides a unified description of both the metallic and localized phases.

In the last decade, it was realized that condensed matter with a gapped spectrum could be in different quantum phases not distinguished by a broken symmetry, but by a topological invariant. Such phase transitions from the so-called topologically trivial to the non-trivial phase have since been observed experimentally. Topological invariants count the number of protected subgap edge modes, bound to a defect or propagating along a boundary. In a topological superconductor, bound Majorana fermions emerge as the zero energy excitations, protected by a gapped bulk spectrum. These Majorana bound states (MBSs) have non-Abelian statistics, and is a promising candidate for a fault-tolerant topological quantum computing platform. The MBSs are described by a real (self-adjoint) wavefuction (field operator), thus rendering the scattering matrix real orthogonal, rather than complex unitary. In this report, we discuss the extension of RMT to account for topological properties.

Random-matrix theory of quantum transport addresses the following questions – (1) What is the ensemble of scattering matrices, and (2) How are transport properties obtained from this? These questions are answered by studying the statistical properties of transmission eigenvalues of nanowire geometry, proximitized by an s-wave superconductor. This forms the simplest setup to study topological superconductivity with Majorana bound states at the ends of the nanowire.

This report is organized as follows. We begin providing some background with quasiparticle excitations in superconductor, and review the Kitaev chain – a paradigmatic model for topological superconductivity in Sec. II B. The

antiunitary symmetries are introduced in Sec. III, following which the tenfold-way classification is described in Sec. IV. The key hypothesis of geometrical correlations is discussed and the energy-level repulsion is studied for the symmetry classes. The circular ensemble of scattering matrices is introduced in Sec. V, and electrical conduction is discussed in Sec. VI. Here, we briefly review an experimental setup involving an s-wave proximitized Rashba nanowire, in an in-plane parallel magnetic field. We conclude in Sec. VII.

This report is inspired by, and based on the reviews[2,3] by Beenakker.

II. TOPOLOGICAL SUPERCONDUCTIVITY

.

A. Superconducting quasiparticles

Fermionic excitations Ψ of a superconductor are Bogoliubov quasiparticles – a coherent superposition of ψ_e (negatively charged, filled state above the Fermi level E_F), and ψ_h (positively charge, empty state below the E_F). Unlike in normal metals, the charge of Bogoliubov quasiparticles are not conserved, and the $\pm 2e$ charge fluctuations are absorbed by the Cooper pair condensate of the superconductor. This is a consequence of particle-hole symmetry (Sec. III A), and expresses the ambiguity that an excited state consists an excess unbound electron, or a Cooper pair with a missing electron.

Bogoliubov quasiparticles can be bound by a magnetic vortex or an electrostatic defect. Particle-hole symmetry requires that the bound state energies come in pairs $\pm E$, with the possibility of an unpaired state at the Fermi level ($E = 0$). This requirement translates into the relation $a_E = a^\dagger_{-E}$ for second-quantized quasiparticle creation/annihilation operators, and the existence of a self-adjoint operator $a_0 = a_0^\dagger$ at the Fermi level. This results in a correspondence between Bogoliubov quasiparticles and Majorana fermions – a particle that is its own antiparticle[4,5].

Majorana fermions emerge as stable bound states at the Fermi level. They can't be displaced from $E = 0$ without breaking particle-hole symmetry, and hence are said to be topologically protected zero modes.

B. Kitaev Chain

Kitaev introduced a toy-model for a one-dimensional superconducting wire, with a tight-binding Hamiltonian given by

$$H = -\mu \sum_n c_n^\dagger c_n - t \sum_n \left(c_n^\dagger c_n + \text{h.c.} \right) + \Delta \left(c_n c_{n+1} + \text{h.c.} \right), \tag{1}$$

where the operator c_n annihilates a spinless fermion at site n. Each site feels a chemical potential μ and adjacent sites are coupled by a hopping term t. The p-wave superconducting pairing Δ couples adjacent sites in the chain.

Each site of the Kitaev chain is associated with a pair of Majorana operators, which is defined as follows

$$\begin{aligned} \gamma_{n1} &= c_n^\dagger + c_n \\ \gamma_{n2} &= i c_n - i c_n^\dagger \end{aligned} \tag{2}$$

The Majorana operators are self-adjoint $\gamma_{ns}^\dagger = \gamma_{ns}$ by construction, and have the anti-commuting relation

$$\gamma_{n's'}\gamma_{ns} + \gamma_{ns}\gamma_{n's'} = 2\delta_{nn'}\delta_{ss'} \tag{3}$$

Inverting the defintion of the Majorana operators (Eq. 2), the Hamiltonian takes the bilinear form

$$H = \sum_{n,m} i \Gamma_n \Gamma_m A_{nm} + \text{const}, \tag{4}$$

where $\Gamma_n = (\gamma_{n1}, \gamma_{n2})$ is a Majorana vector, and A is a real antisymmetric matrix $A = A^* = -A^T$. The methods of RMT would be applied to this matrix A.

It is well known that a real antisymmetric matrix of even dimension can be factored as

$$A = O \begin{bmatrix} 0 & E_1 & 0 & 0 \\ -E_1 & 0 & \ddots & 0 \\ 0 & \ddots & 0 & E_M \\ 0 & 0 & -E_M & 0 \end{bmatrix} O^T, \tag{5}$$

where O is a real orthogonal matrix of dimension $2M$, and E_n's are the positive eigenvalues of A. The rationale behind studying even dimensional A will be motivated in the subsequent section.

The determinant $\det O \in \{-1, +1\}$ and switches sign whenever an eigenvalue E_n crosses zero. The sign of the Pffafian (PfA) is a diagnostic of such zero energy crossings:

$$\begin{aligned} \text{Pf}A &= \det O \prod_n E_n \\ \mathcal{P} &:= \det O = \text{sgn}\text{Pf}A = \pm 1, \end{aligned} \tag{6}$$

The topological quantum number $\mathcal{P}$ gives the fermion parity of the superconducting ground state, with $\mathcal{P} = +1$ ($\mathcal{P} = -1$) denoting the absence (presence) of an unpaired electron. Figure 1 shows the spectrum of a Bogoliubov-deGennes (BdG) Hamiltonian $H(\theta)$ describing a superconductor, with the phase determined by the ground state fermion parity. Here, $H(\theta) = \theta H_0 + (1-\theta)H_1$, with particle-hole symmetric matrices $H_{0,1}$, and a real parameter θ that could, for example, model an external magnetic field. A change in the topological invariant $\mathcal{P}$ indicates a phase transition.

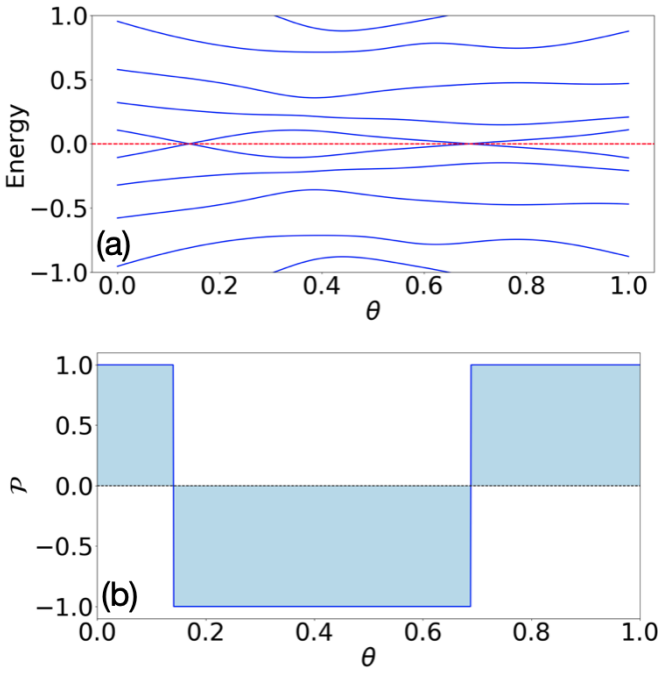

FIG. 1: (a) The energy eigenvalues of $H(\theta) = \theta H_0 + (1-\theta)H_1$, where $H_{0,1}$ are particle-hole symmetric matrices (see Sec. III A) and θ is a real parameter, and (b) the fermion parity corresponding to the spectrum in (a). Each switch of the sign of $\mathcal{P}$ corresponds to a change in the fermion parity.

C. Majorana bound states

As outlined in the previous subsection, each level crossing corresponds to a fermion parity switch, and hence an odd number of such crossings would correspond to a topologically non-trivial phase. A thermodynamic signautre of the same would involve adding periodic boundary conditions to the Kitaev chain and threading a flux quantum ($\Phi_0 = h/2e$) through it. Here, h is Planck's constant and e is the electron charge. A change in the parity $\mathcal{P}$ would correspond to a non-trivial topology:

$$\mathcal{P}(0)\mathcal{P}(h/2e) = \begin{cases} +1 & \text{trivial,} \\ -1 & \text{non-trivial} \end{cases} \tag{7}$$

In a transport setup, one would determine the sign of the reflection matrix from either end. Assuming that transmission is negligible, the reflection matrix is orthogonal, and its determinant would switch sign whenever a reflection eigenvalue crosses zero.

$$Q = \det r = \begin{cases} +1 & \text{trivial,} \\ -1 & \text{non-trivial} \end{cases} \tag{8}$$

This transition is concomitant with the closing of the excitation gap.

III. FUNDAMENTAL SYMMETRIES

The results of RMT are applied to disordered systems with broken symmetries. If a discrete symmetry persists, then the Hamiltonian commutes with a unitary U, and can be block diagonalized in the eigenbasis of U. This unitary symmetry can then be ignored if we restrict our analysis to a single block. However, this cannot be done if the symmetry corresponds to an antiunitary operator, or anti-commutation with a unitary operator. The aforementioned symmetries give rise to particle-hole, time-reversal and chiral symmetries, and are discussed in this section. These additional symmetries are the basis of the so-called "ten-fold way" of Hamiltonian ensembles in RMT.

A. Particle-hole symmetry

The second-quantized mean-field Hamiltonian for a superconductor with s-wave pairing is given by,

$$\mathcal{H} = \hat{\Psi}^\dagger H \hat{\Psi}, \quad \hat{\Psi} = (\hat{\psi}_\uparrow, \hat{\psi}_\downarrow, \hat{\psi}_\uparrow^\dagger, \hat{\psi}_\downarrow^\dagger) \tag{9}$$

where $\hat{\Psi}$ is the 4-Nambu field operator, expressed in terms of the particle-hole field operators, and H is the Bogoliubov-deGennes Hamiltonian

$$H = \begin{bmatrix} H_0 - E_F & -i\sigma_y\Delta \\ i\sigma_y\Delta^* & -H_0^* + E_F \end{bmatrix}, \tag{10}$$

with a Fermi energy E_F, s-wave pairing Δ and electron Hamiltonian H_0. The Pauli-matrix σ operates over the spin-space. Note that H_0 for realistic systems involves spatially varying disorder potentials, due to impurity or boundary scattering. This renders the system non-integrable, and thus is suitable for an RMT analysis.

For every eigenfunction $\hat{\Psi}$ of H with energy $E > 0$, there exists an eigenfunction $\tau_x\hat{\Psi}$ with energy $-E$. Here, τ_x is the Pauli matrix over the particle-hole space. This corresponds to the symmetry

$$H = -\mathcal{C}H\mathcal{C}^{-1} = -\tau_x H^* \tau_x, \tag{11}$$

where $\mathcal{C} = \tau_x\mathcal{K}$ is the charge-conjugation operator and $\mathcal{K}$ the operator for complex conjugation. The charge-conjugation operator is antiunitary and squares to $+1$. The Hamiltonain (Eq. 11) is said to have particle-hole symmetry.

For spin-independent H_0, the Hamiltonian decomposes into two non-interacting blocks acting separately on $(\hat{\psi}_\downarrow, \hat{\psi}_\uparrow^\dagger)$ and $(\hat{\psi}_\uparrow, \hat{\psi}_\downarrow^\dagger)$. The charge conjugation operator then corresponds to $\mathcal{C} = i\tau_y\mathcal{K}$, and $\mathcal{C}^2 = -1$.

B. Time-reversal symmetry

Particle-hole symmetry corresponds to an anti-commuting relation with an antiunitary operator, $H\mathcal{C} =$

$-\mathcal{C}H$. When the Hamiltonian commutes with an antiunitary matrix, we get the time-reversal symmetry $H\mathcal{T} = \mathcal{T}H$. Time-reversal operation should flip the spin $\mathcal{T}\sigma\mathcal{T}^{-}1 = -\sigma$ and the momentum $\mathcal{T}\mathbf{p}\mathcal{T}^{-}1 = -\mathbf{p}$, and the corresponding operator is $\mathcal{T} = i\sigma_y\mathcal{K}$ which squares to -1. The Hamiltonian (Eq. 10) commutes with $\mathcal{T}$ if Δ is real and

$$H_0 = \mathcal{T}H_0\mathcal{T}^{-}1 = \sigma_y H_0^* \sigma_y \tag{12}$$

For real Hamiltonians, $\mathcal{T} = \mathcal{K}$, squaring to $+1$. This 'fake' time-reversal symmetry, supplemented with charge-conjugation (Eq.11) results in

$$H = -\tau_x H \tau_x \tag{13}$$

Such an anti-commutation of the Hamiltonian with a unitary is a chiral symmetry.

C. The Majorana representation

The Majorana representation of the Bogoliubov quasiparticles becomes apparent on a unitary transformation

$$\begin{aligned} H &\to \Omega H \Omega^\dagger, \quad \Omega = \frac{1}{\sqrt{2}}\begin{bmatrix} 1 & 1 \\ i & -i \end{bmatrix} \\ \hat{\Psi} &\to \Omega\hat{\Psi} = \begin{pmatrix} \hat{\psi} + \hat{\psi}^\dagger \\ i\hat{\psi} - i\hat{\psi}^\dagger \end{pmatrix} \end{aligned} \tag{14}$$

This is the Majorana representation of a fermion that Kitaev introduced in Sec. II B. In this basis, the particle-hole symmetry (Eq.11) takes the form

$$\begin{aligned} &\mathcal{C} = \mathcal{K} \\ &H = -\mathcal{C}H\mathcal{C}^{-1} \implies H = -H^* \end{aligned} \tag{15}$$

Thus, the Hamiltonian $H = iA$, where A is a real anti-symmetric matrix. Note that this refers to the four-component BdG Hamiltonian (Eq. 9). The spin-independent block-diagonal Hamiltonian cannot be reduced to an imaginary anti-symmetric matrix under any unitary transformation.

With the Hamiltonian defined as above, the BdG equation renders the field operators self-adjoint. Thus, the Bogoliubov quasiparticles at the Fermi level can be thought of as Majorana fermions.

IV. HAMILTONIAN ENSEMBLES

This background sets us up to discuss a RMT of topological superconductors. As noted earlier, RMT of quantum transport studies the statistical properties of the transmission eigenvalues. In contrast, RMT established by Wigner and Dyson dealt with correlations in the spectral statistics of the system. We begin with this conventional spectral description in terms of Hamiltonian ensembles, and discuss its key ingredient – geometric correlations. The scattering matrix ensemble is a useful description in the transport paradigm, which we discuss in Sec. V.

A. The ten-fold way

The first application of RMT involved only a single ensemble of real Gaussian Hamiltonians. With Dyson's three-fold way in 1962, this grew to include the Gaussian orthogonal, unitary and symplectic ensembles, depending on the Hamiltonian elements being real, complex or quaternion. The nomenclature is based on the matrix that diagonalizes the Hamiltonian. Dyson also realized that the circular orthogonal, unitary and symplectic ensembles obtained on exponentiating the Hamiltonians $S = e^{iH}$ corresponded to 3 of the 10 compact symmetric spaces of differential geometry.

Over the last several decades, the remaining seven ensembles have been realized in a physical context. This was first expanded to 6 by adding chiral symmetry in the context of quantum chromodynamics, and to 10 by including particle-hole symmetry in the context of superconductivity.

The expansion to the so-called "ten-fold" way can be understood as follows

- The antiunitary matrix $\mathcal{T}$ that commutes with the Hamiltonian results in two classes, depending on $\mathcal{T}^2 = \pm 1$. This corresponds to time-reversal symmetry in the absence of particle-hole symmetry.
- The antiunitary matrix $\mathcal{C}$ that anti-commutes with the Hamiltonian results in two classes, depending on $\mathcal{C}^2 = \pm 1$. This corresponds to particle-hole symmetry in the absence of time reversal symmetry.
- The combination of $\mathcal{C}^2 = \pm 1$ and $\mathcal{T}^2 = \pm 1$ results in four classes. This corresponds to particle-hole symmetry with time reversal symmetry.
- The unitary matrix $\mathcal{C}\mathcal{T}$ anti-commutes with the Hamiltonian, and results in two additional symmetry classes, if neither particle-hole nor time-reversal symmetries apply.

The salient properties of the ten ensembles resulting from the aforementioned symmetries are listed in Table I.

B. The Wigner-Dyson ensemble

Wigner and Dyson studied an ensemble of $N \times N$ Hermitian matrices H with a probability distribution

$$P(H) \propto \exp\left[-\beta \operatorname{Tr} V(H)\right], \tag{16}$$

The ensemble is called Gaussian when the potential $V(H) \propto H^2$. This results in independently distributed

	D	BDI	DIII	C	CI	CII	A	AI	AII	AIII
$HC=-CH$, $C^2=$	+1	+1	+1	-1	-1	-1	×	×	×	×
$H\mathcal{T}=\mathcal{T}H$, $\mathcal{T}^2=$	×	+1	-1	×	+1	-1	×	+1	-1	×
$HC\mathcal{T}=-C\mathcal{T}H$	×	✓	✓	×	✓	✓	×	×	×	✓
β	2	1	4	2	1	4	2	1	4	2
α	0	0	1	2	1	3	0	0	0	1
ν	0,1	0,1,2,...	0,1	0	0	0,1,2,...	0	0	0	0,1,2,...
d	1	1	2	1	1	2	1	1	2	1
$S^{-1}=$	S^T (orthogonal)			$\tau_y S^T \tau_y$ (symplectic)			$S^\dagger$ (unitary)			
$S^T=$	×	$+S$	$-S$	×	$+S$	$-S$	×	$+S$	$-S$	S^*

TABLE I: The tenfold way classification of symmetry classes of Hamiltonians H and scattering matrices S at the Fermi level. The classes are distinguished by antiunitary symmetries $\mathcal{C}$ ans $\mathcal{T}$ which square to ± 1, and a chiral symmetry $\mathcal{CT}$. The integer ν counts the number of d-fold degenerate, topologically protected zero modes (Majoranas in class D, BDI and DIII). The repulsion exponents of the energy eigenvalues are denoted by α, and β (see Sec. IV B).

matrix elements, and the ubiquity of the Gaussian ensemble is due to this mathematical convenience. Spectral correlations tend to be independent of V in the large N limit, which is a manifestation of the universality alluded to in Sec. I.

The index $\beta = \{1, 2, 4\}$ counts the number of degrees of freedom in the matrix elements, and corresponds to the Gaussian orthogonal, unitary and symplectic ensembles respectively. In the generalization to Dyson's ten-fold way, $\beta = 2$ applies to a ensembles with broken time reversal symmetry. In the presence of time reversal symmetry with $\mathcal{T}^2 = -1$, we have $\beta = 4$, while $\beta = 1$ corresponds to the fake time reversal symmetry $\mathcal{T}^2 = +1$ for a real Hamiltonian.

One of the goals of RMT is to determine from $P(H)$ the statistics of the eigenvalues $\{E_n\}$ and eigenvectors U of $H = U\mathrm{diag}(\{E_n\})U^\dagger$. Since $P(H)$ depends only on the trace of the potential $\mathrm{Tr}\, V(H) = \sum_n V(E_n)$, it is independent of the eigenvectors. This implies that the eigenvector matrix is uniformly distributed in the orthogonal, unitary and symplectic groups for $\beta = \{1, 2, 4\}$ respectively. In order to study the distribution of $\{E_n\}$, we need the Jacobian relating a volume element $d\mu(H)$ in matrix space to $d\mu(U)dE_n$ in the eigenvector and eigenvalue space. The ensembles of class A, AI and AII, introduced by Wigner and Dyson have distinct power laws $\propto |E_i - E_j|^\beta$ for the probability of a pair of energy levels (E_i, E_j) being close to each other.

In the presence of particle-hole and chiral symmetries, the probability distribution of positive eigenvalues picks up an additional factor describing the repulsion of $E_i > 0$ with the pair of $\pm E_j$. The repulsion of E with $-E$ results in a factor $\prod'_k |E_k|^\alpha$, where $\prod'$ denotes a product over positive eigenvalues, and α is a symmetry class dependent constant. In class C, $\alpha = 2$, whereas $\alpha = 0$ in class D. Thus, there is no repulsion at the Fermi level in class D. This can be seen in Fig. 1(a), where level crossings are avoided away from the Fermi level, but can cross at $E = 0$. This enables fermion parity switching, necessary for the topological transition.

The energy level probability distributions in the ten symmetry classes are given by

$$P(\{E_n\}) \propto \prod_{1=i<j}^{N/d} |E_i - E_j|^\beta \prod_{k=1}^{N/d} \exp\left(-\frac{\pi^2 \beta d E_k^2}{4N\delta^2}\right) \quad \text{in class A, AI, AII} \tag{17}$$

$$P(\{E_n\}) \propto \prod_{k=1}^{'(N-\nu d)/2d} |E_k|^{\alpha+\nu\beta} \exp\left(-\frac{\pi^2 \beta d E_k^2}{4N\delta^2}\right) \times \prod_{1=i<j}^{'(N-\nu d)/2d} |E_i^2 - E_j^2|^\beta, \text{ in the other classes} \tag{18}$$

As defined in Table I, the integer ν counts the number of d-fold degenerate, topologically protected zero modes. The density of states in classes D, C and CI are plotted in Fig. 2.

The distribution has the form of a Gibbs distribution in statistical mechanics,

$$P(\{E_n\}) \propto \exp\left[-\beta\left(\sum_{i<j}{}' u(E_i, E_j) + \sum_i{}' V(E_i) + \sum_i{}' w(E_i)\right)\right], \tag{19}$$

where the primed summation is over positive energies; $V(E_i) \propto E_i^2$; the repulsion between $|E| \neq |E'|$

$$u(E, E') = \begin{cases} -\ln|E - E'|, \\ \quad \text{in class A, AI and AII} \\ -\ln|E - E'| - \ln|E + E'|, \\ \quad \text{in the other classes} \end{cases} \tag{20}$$

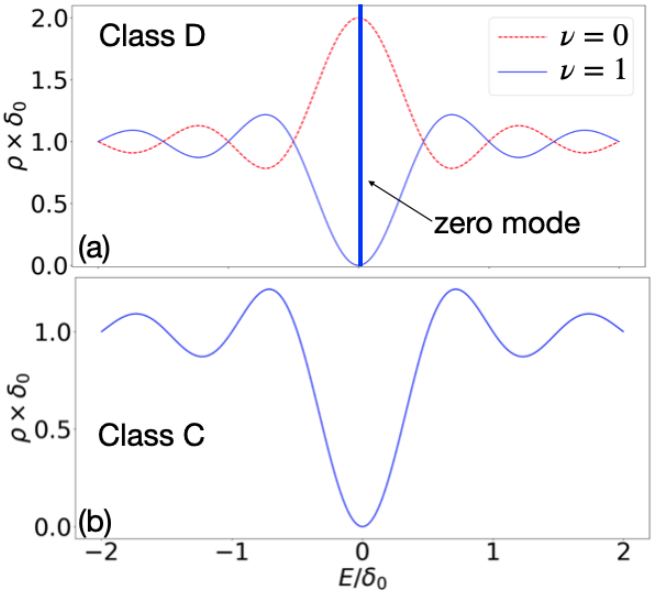

FIG. 2: The numerically computed ensemble-averaged density of states in classes (a) D, (b) C, following Mi et al.[6]. A singular zero mode is depicted for class D, $\nu = 1$. Except for class D with $\nu = 0$, the density of states at the Fermi level vanishes as $|E|^{\alpha+\nu\beta}$.

and the repulsion between E and $-E$

$$w(E) = \begin{cases} 0, & \text{in class A, AI and AII} \\ -\left(\frac{\alpha}{\beta} + \nu\right) \ln|E|, & \text{in the other classes} \end{cases} \tag{21}$$

Expressed in this form, the distribution resembles a Coulomb gas of particles on a line, with a repulsion given by a logarithmic pair potential u, a self energy w and a confinement potential V. This analogy is due to Wigner and Dyson, and it helps in building an intuition.

C. Geometrical correlations

The geometrical character of the spectral correlations is the fundamental hypothesis of the Winger-Dyson ensemble. This implies correlations between the eigenvalues are only due to the Jacobian which relates a volume element in the Hermitian matrix space to the eigenvector and eigenvalue space. This results in the logarithmic repulsion in the eigenvalue distribution. Any other source of correlations between the energy levels would manifest in the departure from a logarithmic pair potential repulsion. Microscopic features of the system enter the potential V, and hence do not affect the energy correlations in the large N limit.

The Wigner-Dyson ensemble was used to study the electronic properties of small metal grains, by Gor'kov and Eliashberg[7]. This was theoretically justified by Efetov's supersymmetric field theory, and the energy-level correlation functions obtained from that matched the Wigner-Dyson ensemble. A few years later, Altshuler and Shklovskii[8] showed that for $|E - E'|$ greater than the Thouless energy E_{th}, the correlations deviates from RMT. For $|E - E'| \gg E_{th}$, the interaction potential decays as a power law and becomes weakly attracting in three dimensions.

The Wigner-Dyson ensemble doesn't just apply to an ensemble of disordered systems, but also to any quantum-mechanical system that is chaotic. The necessary requirement is that there are no unitary symmetries in the system, other than time-translation. Thus, energy is the only constant of motion. An ensemble could consist of a collection of systems, differing in disorder realizations. Alternatively, one could consider a single disordered system and replace the ensemble average over a spectral average over the energy levels. This is more convenient for experimentalists and the equivalence of the two averages is guaranteed by the assumption of ergodicity.

V. SCATTERING MATRIX ENSEMBLES

The scattering theory of transport was pioneered by Landauer[9,10] and Büttiker[11,12]. It is a complete description of transport in the linear response regime, when electron-electron interactions can be neglected. A mesoscopic conductor can be modelled as a phase-coherent disordered region connected by ideal leads. The leads are a representation of a macroscopic thermal bath in the grand canonical ensemble with an equilibrium temperature T and chemical potential μ (or Fermi energy E_F). A difference in T or μ of two or more leads would bias the conductor and result in a non-equilibrium current flow (we do not consider equilibrium current flow in phase-biased Josephson junctions[13] in this report). Scattering in the disordered region is assumed to be elastic, while all inelastic processes occur in the leads.

Consider the disordered mescoscopic conductor, with a set of incident ψ_n^{in} and emitted ψ_n^{out} wavefunction amplitudes, with $n = 1, \ldots, N$ linearly related by

$$\psi_n^{out}(E) = \sum_{m=1}^{N} S_{nm} \psi_m^{in}(E), \tag{22}$$

where S is the scattering matrix with a block structure in the left-right basis

$$S = \begin{bmatrix} r & t' \\ t & r \end{bmatrix} \tag{23}$$

with $N \times N$ reflection matrices r, r' (from left to left and right to right), and transmission matrices t and t' (from left to right and right to left), encoding normal, Andreev as well as crossed-Andreev processes (Sec. VI C). Since scattering is elastic, and conservative, $S^{-1} = S^\dagger$ is unitary, and the four Hermitian matrices $tt^\dagger$, $t't'^\dagger$, $1 - rr^\dagger$ and $1 - r'r'^\dagger$ have identical transmission eigenvalues T_n, which are real numbers $\in [0, 1]$. Note that T_n's different from 0 are 1 are two-fold degenerate by Béri degeneracy[14].

A. Fundamental Symmetries

The Cayley transform

$$S = \frac{1 - i\pi K(E)}{1 + i\pi K(E)}, \quad K(E) = W^\dagger \frac{1}{E - H} W \tag{24}$$

relates the scattering matrix to the Green's function $(E - H)^{-1}$ via broadband coupling matrices W. We assume that W commutes with both the charge conjugation operator $\mathcal{C}$, and time-reversal operator $\mathcal{T}$.

Particle-hole symmetry $H = -\mathcal{C}H\mathcal{C}^{-1}$ translates into

$$S(-E) = \mathcal{C}S(E)\mathcal{C}^{-1} = \begin{cases} S^*(E) & \text{if } \mathcal{C} = \tau_x\mathcal{K} \\ \tau_y S^*(E)\tau_y & \text{if } \mathcal{C} = i\tau_y\mathcal{K} \end{cases} \tag{25}$$

At the Fermi level $E = 0$, this means that $S \in O(N)$ is a real orthogonal matrix for $\mathcal{C}^2 = +1$, and $S \in \mathrm{Sp}(N)$ is a unitary symplectic matrix for $\mathcal{C}^2 = -1$.

Time-reversal symmetry translates into

$$S(E) = \mathcal{T}S(E)\mathcal{T}^{-1} = \begin{cases} S^T(E) & \text{if } \mathcal{T} = \mathcal{K}, \\ \sigma_y S^T(E)\sigma_y & \text{if } \mathcal{T} = i\sigma_y\mathcal{K}, \end{cases} \tag{26}$$

where the superscript T denotes transpose. Changing the basis of outgoing modes such that $S \to i\sigma_y S$, the above condition can be succinctly expressed as

$$S(E) = \pm S^T(E), \tag{27}$$

for $\mathcal{T}^2 = \pm 1$ respectively. Finally, the chiral symmetry translates into

$$S(E) = \mathcal{C}\mathcal{T}S^\dagger(-E)(\mathcal{C}\mathcal{T})^{-1} \tag{28}$$

B. Circular ensembles

As mentioned in Sec. IV C, the random-matrix theory is applicable in systems with chaotic dynamics. The notion of chaos in classical systems is well defined in terms of motion trajectories with Lyapunov exponents for an infinitesimal change in the initial conditions. In quantum mechanics, the dynamics are governed by a linear Schrödinger equation with unitary evolution. The concept of chaos was translated to the ensemble of scattering matrices – at fixed energy – that was produced on infinitesimal perturbations of the disorder in the system. Chaotic scattering, then refers to uniformly distributed scattering matrices in the unitary group

$$P(S) = \text{constant}, \quad S \in U(N) \tag{29}$$

This is referred to as the circular unitary ensemble (CUE) of scattering matrices, and describes transport in a chaotic quantum system with broken time reversal symmetry ($\beta = 2$). It has found applications in the context of microwave cavities[15] and quantum dots[2].

In the presence of time-reversal symmetry with $\mathcal{T}^2 = 1$ (Eq. 26), S is constrained to be of the form $S = UU^T$, where U is uniformly distributed in $U(N)$. This is referred to as the circular orthogonal ensemble (COE), because unitary symmetric matrices form the coset $U(N)/O(N)$ of the orthogonal group.

For time-reversal symmetry with $\mathcal{T}^2 = -1$, the scattering matrix takes the form $S = U\sigma_y U^T\sigma_y$, with U uniformly distributed in $U(N)$ for even N. This is referred to as the circular symplectic ensemble (CSE), because S is in the coset $U(N)/Sp(N)$ of the unitary symplectic group.

C. Majorana circular ensembles

Superconductivity induces particle-hole correlations at the interface with a normal metal, via a process known as Andreev reflections. This involves the conversion of a particle-like excitation at energy $E_F + E$, into a hole-like excitation at energy $E_F - E$, and the transfer of Cooper pair to the superconducting condensate. As described in Sec. III C a linear superposition of particle and hole-like quasiparticles at the Fermi level ($E \to 0$) results in a self-conjugate (self-adjoint) Majorana wavefunction (field operator).

Andreev scattering doesn't conserve charge, however, quasiparticle number is conserved. Thus, the scattering matrix continues to be unitary. Furthermore, the reality of the Majorana wavefunctions constraints the scattering matrix $S(E = 0)$ to the real orthogonal subgroup,

$$P(S) = \text{constant}, \quad S \in O(2N), \tag{30}$$

with a dimension $2N$ to accommodate for the electron and hole degrees of freedom. This is referred to as the circular real ensemble (CRE), or the Haar-orthogonal matrix[16].

The restriction to $S = \pm S^T$ (Eq. 27) within the orthogonal group produces to further ensembles – T_+CRE (symmetry class BDI), and T_-CRE (symmetry class DIII). Time-reversal symmetry ($\mathcal{T} = i\sigma_y\mathcal{K}$) results in T_-CRE, whereas chiral symmetry ($\mathcal{T} = \mathcal{K}$) is responsible for T_+CRE.

In Table II, we summarize the three scattering ensembles that support Majorana zero modes.

D. Topological quantum numbers

The three ensembles in Table II, in turn consist of disjoint subensembles characterized by an integer Q known as the "topological quantum number", or topological invariant.

In CRE, the two subensembles correspond to $S \in O_\pm(2N)$, where $O_\pm$ is the orthogonal subgroup with determinant ± 1. Thus, the topological invariant

$$Q = \det S = \pm 1, \quad \text{(CRE)} \tag{31}$$

Ensemble	CRE	T_+CRE	T_-CRE
Symmetry class	D	BDI	DIII
S-matrix elements	Real	Real	Real
S-matrix space	Orthogonal	Orthogonal symmetric	Orthogonal anti-symmetric
Topological invariant	$\det S$	$\frac{1}{2}\operatorname{Tr} S$	PfS

TABLE II: The three ensembles that support Majorana zero modes

In T_-CRE, the scattering matrix can be expressed as

$$S = OJO^T, \quad J = \begin{bmatrix} 0 & \mathbb{I}_N \\ -\mathbb{I}_N & 0 \end{bmatrix}, \tag{32}$$

where $\mathbb{I}_N$ is the $N\times N$ identity matrix, and O is uniformly distributed in $O_\pm(2N)$, producing the two subensembles. They can be distinguished by the Pfaffian of S

$$\begin{aligned} Q = \mathrm{Pf}S &= (\mathrm{Pf}J)\det O \\ &= (-1)^{N(N-1)/2}\det O = \pm 1, \quad (T_-\mathrm{CRE}) \end{aligned} \tag{33}$$

Finally, the T_+CRE ensemble of symmetric orthogonal scattering matrix can be decomposed as

$$S = O\Sigma O^T, \quad \Sigma = \mathrm{diag}(\pm 1, \ldots, \pm 1), \tag{34}$$

where $O \in O_+(2N)$ without loss of generality, and Σ is known as the "signature matrix". The trace of the scattering matrix defines the topological invariant

$$\begin{aligned} Q = \frac{1}{2}\operatorname{Tr} S &= \frac{1}{2}\operatorname{Tr}\Sigma \\ &= N - \nu(S) = 0, \pm 1, \ldots, \pm N, \quad (T_+\mathrm{CRE}), \end{aligned} \tag{35}$$

where $\nu(S)$ is the number of -1 eigenvalues of S.

The topological quantum number Q of D and DIII are called $\mathbb{Z}_2$ invariants, since it can take only two values. Class BDI has a $\mathbb{Z}$ topological number, because it can take any integer value.

VI. ELECTRICAL CONDUCTION

A. Majorana nanowire

The most popular physical realization of the Kitaev chain toy model involves a III-V semiconductor nanowire, in proximity to an s-wave superconductor. A semiconductor nanowire (InAs/InSb) is proximitized by an s-wave superconductor (Al/Nb), and tunnel coupled to gold leads. Above a critical in-plane parallel magnetic field, a pair of Majorana fermion are bound to the ends of the nanowire. The Hamiltonian of this system is of the form Eq. 10, with

$$H_0 = \frac{\mathbf{p}^2}{2m_{\mathrm{eff}}} + U(\mathbf{r}) + \alpha_{so}\left(\sigma_x p_y - \sigma_y p_x\right) + \frac{1}{2}g^{\mathrm{eff}}\mu_B B\sigma_x, \tag{36}$$

where $\mathbf{p} = -i\partial/\partial\mathbf{x}$ is the momentum operator, m_{eff} is the effective mass, and $U(\mathbf{r})$ is the spatially varying potential energy. The spin is coupled to the momentum in the x-y plane via the Rashba spin-orbit coupling. This breaks spin-rotation symmetry. An in-plane parallel magnetic field $\mathbf{B} = B\hat{\mathbf{x}}$ breaks time reversal symmetry and results in a Zeeman splitting $E_Z = (1/2)g^{\mathrm{eff}}\mu_B B \approx 1$ meV at $B = 1$ T.

Lutchyn et al.[17], and Alicea et al.[18], discovered that the nanowire enters the topological superconducting phase, with Majorana bound states at the ends, when the Zeeman energy exceeds the superconducting pair potential induced by the proximity effect. This prediction has been the basis of the experimental effort over the last decade, and the development of RMT for the same.

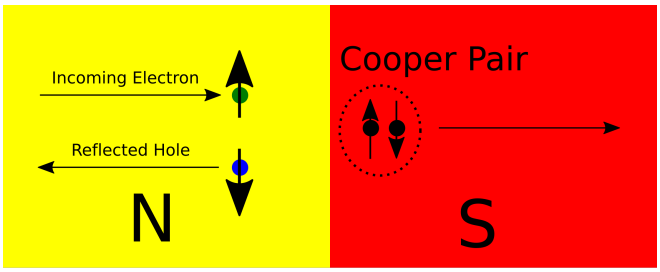

FIG. 3: The process of Andreev reflection at the normal (N)-superconductor (S) interface is depicted as the retroreflection of an up-spin electron into a down-spin hole.

B. Signature of Majorana modes

The topological quantum number Q counts the number ν of Majorana modes at each end of the wire. This number can be determined from the reflection matrix r at one end of the nanowire.

The reflection matrix is unitary if the nanowire is long enough that transmission can be neglected. In the particle-hole Nambu basis

$$r = \begin{bmatrix} r_{ee} & r_{eh} \\ r_{he} & r_{hh} \end{bmatrix}, \tag{37}$$

where each of the submatrices are $N\times N$, with r_{ee}, r_{hh} the

reflection amplitudes for normal reflection, and r_{eh}, r_{he} the Andreev reflection (Fig. 3) amplitudes.

The particle-hole symmetry of classes D and BDI is expressed as $r = \tau_x r^* \tau_x$, while chiral symmetry of class BDI is $r = r^T$. This corresponds to

$$\begin{aligned} r_{ee} &= r_{hh}^*, \quad r_{eh} = r_{he}^*, \text{ (class D and BDI)} \\ r_{ee} &= r_{hh}^T, \quad r_{he} = r_{he}^\dagger, \text{ (class BDI only)} \end{aligned} \tag{38}$$

The condition of unitarity, in addition to particle-hole symmetry ($r = \tau_x r^* \tau_x$) implies that the determinant of r is real, and hence equal to ± 1. In the BDI class, $(\tau_x r)^2 = \mathbb{I}_{2N}$, and thus its $2N$ eigenvalues are all ± 1. The topological invariants can thus be expressed as properties of the reflection matrix

$$\begin{aligned} &Q = \det r = \pm 1, \quad \nu = \frac{1}{2}(1 - Q), \text{ in class D and DIII} \\ &Q = \frac{1}{2}\operatorname{Tr}(\tau_x r) = \operatorname{Tr} r_{he} \in \{0, \pm 1, \ldots, \pm N\}, \\ &\nu = |Q|, \text{ in class BDI} \end{aligned} \tag{39}$$

C. Conductance distribution

The linear response conduction in the nanowire geometry can be determined in terms of the Andreev reflection amplitudes as

$$G/G_0 = 2 \operatorname{Tr} r_{he} r_{he}^\dagger = 2 \sum_{n=1}^{N} A_n, \tag{40}$$

where $G_0 = e^2/h$ is the conductance quantum, and A_n are the Andreev reflection eigenvalues. The factor of two accounts for the charge of $2e$ transferred for every Andreev reflection at the normal-superconductor interface. Thus, we observe that both the conductance and the number of Majorana modes are given by the same reflection matrix. The Béri degeneracy[14] enforces upper and lower bounds on the conductance

$$2\nu \leq G/G_0 \leq 2(N - \zeta), \tag{41}$$

where $\zeta = 0$ ($\zeta = 1$) if $N - \nu$ is even (odd).Thus, for $N > 1$, the conductance is not uniquely determined ν. Assuming a circular ensemble for r, a statistical dependence of G on ν can be derived.

Among the N eigenvalues of $r_{he} r_{he}^\dagger$, ν are pinned to 1, and ζ are pinned at 0. The remaining two-fold degenerate A_n's can take values in $(0, 1)$. The distribution of A_n's for the symmetry classes D and BDI are given by

$$\begin{aligned} P_{\mathrm{D}}(\{A_n\}) &\propto \prod_{1=i<j}^{M} (A_i - A_j)^4 \prod_{k=1}^{M} A_k^{2\zeta} (1 - A_k)^{2\nu}, \\ P_{\mathrm{BDI}}(\{A_n\}) &\propto \prod_{1=i<j}^{M} (A_i - A_j)^2 \prod_{k=1}^{M} A_k^{\zeta - 1/2} (1 - A_k)^{\nu}, \end{aligned} \tag{42}$$

where $M = \frac{1}{2}(N - \nu - \zeta)$. The resulting distribution of conductance for $N = 3$, in each of the symmetry classes is shown in Fig. 4. It is interesting to note that as N increases, the conductance distribution $P(G)$ becomes less sensitive to the presence of a Majorana mode. In fact, for $N > p$, the p^{th} cumulant of $P(G)$ becomes completely independent of ν.

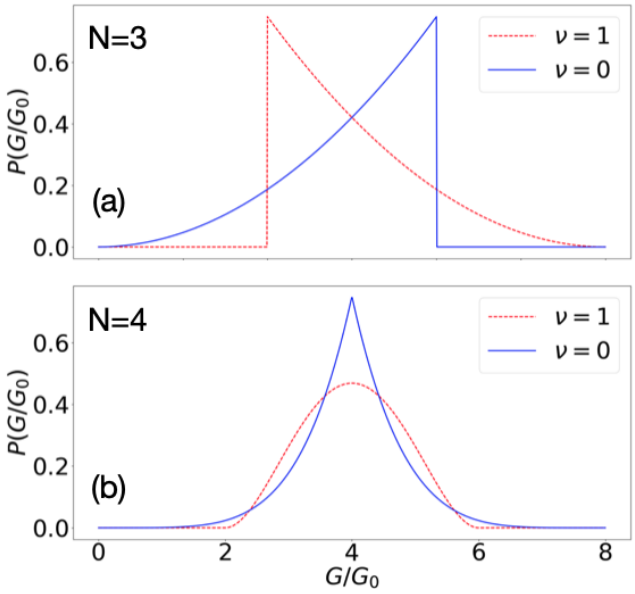

FIG. 4: Probability distribution of the conductance for $N = 3$ modes, in CRE of class D, with ($\nu = 1$, red) and without ($\nu = 0$, blue) a zero mode, following Beenakker et al.[19]. The curves are obtained by integrating the probability distribution of Andreev refelction eigenvalues, and hence are the results from random-matrix theory.

D. Experimental signatures of Majorana modes

1. *Weak antilocalization*

Counting the number of Majorana zero modes in terms of topological invariants builds a strong theoretical framework, but the reflection matrix cannot be explicitly measured in an experiment. The presence or absence of a Majorana bound state is a topological property of the system, and hence its Andreev reflection amplitude at the Fermi level should be pinned at 1, irrespective of whether or not the nanowire is tunnel coupled to the leads. A tunnel-barrier implemented via a quantum point contact would results in a zero-bias conductance peak. Since 2012, there have been several reports of this resonant quantized zero bias conductance peak in proximitized nanowire geometries.

Meanwhile, it was also realized that topologically trivial nanowires could also have a zero bias conductance peak arising from the weak-antilocalization effect.

This resuts from the constructive interference of phase-conjugate scattering sequences (see Fig. 5). In normal metals, this requires time-reversal symmetry, however, the particle-hole symmetry of a superconductor can support this effect via Andreev reflections. A numerical sim-

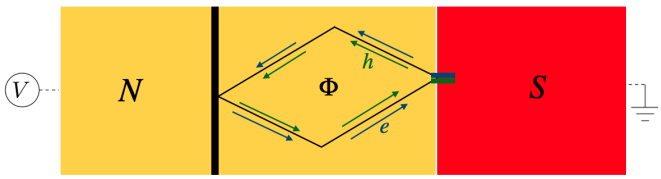

FIG. 5: An example of constructive interference between phase-conjugate series of scattering events responsible for weak antilocalization in an NS junction. Mediated by Andreev reflections, the electron and hole encircle the same flux. but carry opposite charge. Hence, the total phase accumulated vanishes and the interference is constructive. Adapted from Refs[3,20]

ulation of the zero bias peak from a Majorana mode and weak-antilocalization is shown in Fig. 3 of Ref[20]. The two peaks can be compared in a random-matrix theory, by including the effect of the tunnel barrier on the circular ensemble of reflection matrices. A tunnel barrier, parameterized by the transmission probability T per mode, transforms the relfection matrix r

$$r \to \sqrt{1-T} + Tr\left(1+\sqrt{1-T}r\right)^{-1} \tag{43}$$

This results in a non-uniform distribution, known as the Poisson kernel of the circular ensemble

$$P(r) \propto |\det\left(1-\sqrt{1-T}r\right)|^{-p}, \tag{44}$$

where $p = 4N$ in the CUE, and $p = 2N-1$ in CRE.

Now, for reflection matrices at the Fermi level, we take r to be uniformly distributed in $O_+(2N)$ for the topologically trivial system, and in $O_-(2N)$ for the non-trivial system. Away from the Fermi-level, the constrains of reality does not hold, and the reflection matrices are uniformly distributed over the entire unitary group $U(2N)$. Thus, the peak height can be obtained by

$$\delta G = \langle G\rangle_{\mathrm{CRE}} - \langle G\rangle_{\mathrm{CUE}} \tag{45}$$

where the averages are over the conductance distributions in the CRE and CUE ensembles of the reflection matrix. Results are shown in Fig. 6

2. *Andreev resonances*

While weak antilocalization results in the disorder-averaged zero bias conductance peak in trivial nanowires, certain sample specific peaks at zero bias have also been observed (Fig). Andreev resonances with quasibound low energy states are responsible for these peaks in trivial

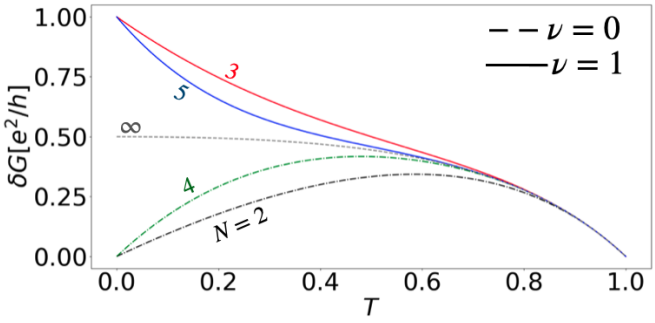

FIG. 6: The amplitude of the zero-bias conductance peaks are computed as a function of the tunneling probability T, for the symmetry class D, following Pikulin et al.[21]. The dashed and solid lines represent the topologically trivial (even N) and non-trivial (odd N) regimes respectively. The peak doesn't depend on ν, as $N \to \infty$.

nanowires. In the the voltage bias - magnetic field plot of the conductance, these appears as an X – a pair of resonant peaks meet and split again, or a Y – the pair of resonant peaks remain pinned at zero bias over a range of magnetic fields.

The poles of the reflection matrix encode the center and width of these Andreev resonances. From the Cayley transform (Eq. 24), the scattering matrix can be expressed in terms of the lead-wire broadband coupling matrix W

$$r(E) = 1 - 2\pi i W^\dagger \left(E - H + i\pi W W^\dagger\right)^{-1} W. \tag{46}$$

The poles of this reflection matrix occur at the eigenvalues of the non-Hermitian Hamiltonian of the open system

$$\mathcal{H} = H - i\pi W W^\dagger. \tag{47}$$

The positive definiteness of the coupling matrix product $WW^\dagger$ constraints all poles to lie in the lower half of the complex plane, and the particle-hole symmetry requires that poles occur in pairs $(\epsilon, -\epsilon^*)$.

For a tunnel barrier with a broadband transmission T, the coupling matrix W is given by

$$\begin{aligned} W_{nm} &= w_n \delta_{nm}, \quad 1 \le n \le N, \quad 1 \le m \le 2N \\ |w_n|^2 &= \frac{N\delta_0}{\pi^2 T}\left(2 - T - 2\sqrt{1-T}\right), \end{aligned} \tag{48}$$

where δ_0 is the typical energy level spacing.

For $|\operatorname{Re}\epsilon| > \delta_0$ the real part of the pole has a uniform distribution. For smaller $|\operatorname{Re}\epsilon|$, the poles are repelled from the imaginary axis in class C, while they accumulate on the same for class D.

Note that a non-degenerate pole on the imaginary axis is robust, since it cannot acquire a non-zero real part without breaking particle-hole symmetry. Now, in class C, the antiunitary operator $\mathcal{C}$ squares to -1. Thus, by Kramer's theorem, every pole is two-fold degenerate and

robust poles on the imaginary axis do not exist. However, the charge-conjugation operator $\mathcal{C}$ squares to $+1$ in class D. Here, Kramer's theorem doesn't hold, and hence there persists a number N_Y of non-degenerate robust poles on the imaginary axis.

The reflection matrix is orthogonal at the Fermi level, with a determinant depending on the parity of N_Y

$$(-1)^{N_Y} = \lim_{E\to 0} \det r(E) = Q, \tag{49}$$

and hence, the nanowire is in the topologically non-trivial phase for odd N_Y. The topological phase transition involves a change in N_Y by ± 1, and the closing of the excitation gap. The trivial pole transition, however, maintains the parity of N_Y (changes by ± 2), and the excitation gap doesn't close. Though these are two very different physical processes, the conductance signature is an identical Y-shaped resonance. The average number N_Y was calculated[6] to be

$$\langle N_Y \rangle \approx T^{3/2}\sqrt{N}, \tag{50}$$

for $T \ll 1$. Thus, a way to suppress trivial ± 2 pole transitions is to have a low number of semiconductor modes coupled to the superconductor, with a small tunnel coupling T. Moreover, the pole transition is a sample-specific effect, while the topological transition is a robust and should survive a disorder-average. Finally, the ± 2 trivial pole transitions measure from either end of the nanowire would be uncorrelated to each other, whereas correlated quantized peaks would be observed from either end in a Majorana nanowire.

VII. CONCLUSION

In this report, we reviewed the framework of random-matrix theory and its application to topological condensed matter systems. In particular, we focused topological invariants involving fermion parity switches leading to the emergence of Majorana zero modes.

The tenfold-way is an exhaustve classification of the symmetr classes of non-interacting fermions. Three of these classes (D, BDI and DIII) support Majorana modes. We discussed the scattering matrix ensembles for the aforementioned symmetry classes. The phase of the system is determined by the topological quantum number, and we outlined how the same can be determined from the reflection matrix.

Finally, we used this to study the most ubiquitous experimental signature for Majorana bound states – the zero-bias conductance peak. A Rashba nanowire setup was briefly discussed and the origin of trivial zero-bias conductance peaks from weak-antilocalization and Andreev resonances was outlined.

While this is a seemingly complete description of the topological phases in single-particle, more recent work aims at a similar classification for interacting systems. It would be interesting to see if the techniques of RMT can be extended to the same.

[1] L. Nemes, Acta Physica Hungarica **73**, 95 (1993), URL https://doi.org/10.1007/BF03054187.

[2] C. W. J. Beenakker, Rev. Mod. Phys. **69**, 731 (1997), URL https://link.aps.org/doi/10.1103/RevModPhys.69.731.

[3] C. W. J. Beenakker, Rev. Mod. Phys. **87**, 1037 (2015), URL https://link.aps.org/doi/10.1103/RevModPhys.87.1037.

[4] E. Majorana and L. Maiani, *A symmetric theory of electrons and positrons* (Springer Berlin Heidelberg, Berlin, Heidelberg, 2006), pp. 201–233, ISBN 978-3-540-48095-2, URL https://doi.org/10.1007/978-3-540-48095-2_10.

[5] E. Majorana, Il Nuovo Cimento (1924-1942) **14**, 171 (2008), URL https://doi.org/10.1007/BF02961314.

[6] S. Mi, D. I. Pikulin, M. Marciani, and C. W. J. Beenakker, Journal of Experimental and Theoretical Physics **119**, 1018 (2014), URL https://doi.org/10.1134/S1063776114120176.

[7] L. P. Gor'kov and G. M. Eliashberg, SOVIET PHYSICS JETP-USSR **21**, 940 (1965).

[8] B. L. Altshuler and B. I. Shklovskii, SOVIET PHYSICS JETP-USSR **64**, 127 (1986).

[9] R. Landauer, IBM Journal of Research and Development **1**, 223 (1957).

[10] R. Landauer, Zeitschrift für Physik B Condensed Matter **68**, 217 (1987), URL https://doi.org/10.1007/BF01304229.

[11] M. Büttiker, Phys. Rev. Lett. **57**, 1761 (1986), URL https://link.aps.org/doi/10.1103/PhysRevLett.57.1761.

[12] M. Buttiker, IBM Journal of Research and Development **32**, 317 (1988).

[13] B. Josephson, Physics Letters **1**, 251 (1962), ISSN 0031-9163, URL http://www.sciencedirect.com/science/article/pii/0031916362913690.

[14] B. Béri, Phys. Rev. B **79**, 245315 (2009), URL https://link.aps.org/doi/10.1103/PhysRevB.79.245315.

[15] H. Stöckmann, *Quantum Chaos: An Introduction* (Cambridge University Press, Cambridge, England, 2007).

[16] M. Pozniak, K. Zyczkowski, and M. Kus, Journal of Physics A: Mathematical and General **31**, 1059 (1998), URL https://doi.org/10.1088%2F0305-4470%2F31%2F3%2F016.

[17] R. M. Lutchyn, J. D. Sau, and S. Das Sarma, Phys. Rev. Lett. **105**, 077001 (2010), URL https://link.aps.org/doi/10.1103/PhysRevLett.105.077001.

[18] J. Alicea, Y. Oreg, G. Refael, F. von Oppen, and M. P. A. Fisher, Nature Physics **7**, 412 EP (2011), URL https:

//doi.org/10.1038/nphys1915.

[19] C. W. J. Beenakker, J. P. Dahlhaus, M. Wimmer, and A. R. Akhmerov, Phys. Rev. B **83**, 085413 (2011), URL https://link.aps.org/doi/10.1103/PhysRevB.83.085413.

[20] D. I. Pikulin, J. P. Dahlhaus, M. Wimmer, H. Schomerus, and C. W. J. Beenakker, New Journal of Physics **14**, 125011 (2012), URL https://doi.org/10.1088%2F1367-2630%2F14%2F12%2F125011.

[21] D. I. Pikulin and Y. V. Nazarov, JETP Letters **94**, 693 (2012), URL https://doi.org/10.1134/S0021364011210090.